Present Efficiencies and Future Opportunities in Thermophotovoltaics

Tobias Burger, Caroline Sempere, Bosun Roy-Layinde, Andrej Lenert*
Chemical Engineering, University of Michigan, Ann Arbor, MI 48109, United States
Corresponding author email: alenert@umich.edu

Abstract

Despite the relevance of thermophotovoltaic (TPV) conversion to many emerging energy technologies, identifying which aspects of current TPV designs are favorable and where opportunities for improvement remain is challenging because of the experimental variability in TPV literature, including emitter and cell temperatures, cavity geometry, and system scale. This review examines several decades of experimental TPV literature and makes meaningful comparisons across TPV reports by comparing each energy conversion step to its respective, experiment-specific thermodynamic limit. We find that peak reported efficiencies are nearing 50% of their thermodynamic limit. Emitter-cell pairs that best manage the broad spectrum of thermal radiation exhibit the best efficiencies. Large gains in peak efficiency are expected from further suppression of sub-bandgap radiative transfer, as well as improvements in carrier management that address poor bandgap utilization and Ohmic losses. Furthermore, there is a noticeable practical gap between the leading material pairs and integrated devices, mainly due to a lack of scaled-up high-performance materials, which exposes surfaces to parasitic heat loss. Provided these challenges are overcome, TPVs may ultimately provide power on demand and near the point-of-use, enabling greater integration of intermittent renewables.

Introduction

Thermophotovoltaic (TPV) generators utilize the photovoltaic effect to convert heat into electrical power (Fig. 1). Many potential heat sources can be interfaced with TPVs, including combustion of fossil fuels, nuclear power, concentrated solar thermal, variable renewable electricity, and high-temperature waste heat streams. As heat is supplied to the thermal emitter, it drives radiative emission to the cold-side photovoltaic cell. Absorption of high-energy (in-band) photons in the cell excites electron-hole pairs, while low-energy (out-of-band) thermal radiation may be suppressed or reflected to minimize the heat input. Ultimately, photoexcited carriers are separated, inducing a voltage across the junction that drives current across a load.

Thermophotovoltaic conversion is a promising approach for a variety of energy applications. TPV generators can provide silent power generation near the point-of-use using a range of heat sources, offering advantages over existing generators and conventional power cycles. In this way, low-grade heat generated as a byproduct could be used for domestic hot water and space heating.^{1–3} Furthermore, TPVs may enable high-temperature thermal battery approaches for grid-scale storage of electricity that are expected to have superior energy density and cost metrics compared to electrochemical batteries.^{4,5}

The efficiency of TPV-based energy systems is largely dependent on how effectively energy losses are mitigated at each conversion step. Important loss pathways include emission and absorption of out-of-band photons, thermalization of in-band photons, electron-hole pair recombination, Ohmic losses along the current conduction pathway, and parasitic heat losses to the surroundings. Presently, TPVs may be suitable for application in space exploration, which requires high specific power (W/kg), and remote power generation.⁶ However, broader applications, such as distributed combined heat and power, ^{1–3} grid-scale energy storage, ^{4,5} waste heat recovery, ⁷ and direct solar energy conversion, ^{8–14} necessitate improvements in cost and conversion efficiency.

To accelerate the development of TPVs and realize efficiencies closer to theoretical limits, it is important to identify which aspects of current designs are favorable and where significant technological gaps remain. However, meaningfully comparing experimental TPV literature is challenging because of the variability in emitter and cell temperature and cavity geometry. Consequently, comparison of metrics such as short-circuit current density (J_{sc}) and open-circuit

voltage (V_{oc}) alone, which is meaningful in the solar PV literature, ¹⁵ is poorly suited for evaluation of TPV performance.

To overcome this barrier, we review current approaches and identify major opportunities for future research by comparing leading TPVs across material systems to thermodynamic limits. We account for variable testing conditions by comparing major energy conversion steps to their respective fundamental limit, calculated using experiment-specific parameters such as bandgap (E_g), emitter temperature (T_h), and cell temperature (T_c). This limit is defined by the detailed-balance model that considers radiative recombination as the lone carrier loss mechanism (i.e., the radiative limit). ^{9,16,17} By accounting for these effects, we can make systematic comparisons across reported efficiencies and identify limitations in spectral and carrier management within leading TPV pairs. Although systematic reviews of the literature have been conducted, notably the work of Mauk, ¹⁸ Zhou, *et al.*, ¹² Datas, *et al.*, ⁶ Ferrari, *et al.*, ¹⁹ Daneshvar, *et al.*, ²⁰ and Sakakibara, *et al.*, ²¹ an analysis of how the performance metrics of leading TPVs compare to the radiative limit has not been reported. We then discuss and rationalize the efficiency gap observed when scaling up and translating TPV emitter-cell pairs toward practical implementation.

Our review is structured as follows. Section 1 defines the figures of merit used to compare experimental TPV literature. Section 2 analyzes leading TPV emitter-cell pairs and identifies current limitations in spectral and carrier management. Sections 3 and 4 provide a review of leading and emerging component-wise approaches for improvement of spectral and carrier management, respectively. Section 5 discusses the efficiency gap observed between TPV emitter-cell pairs and more scaled-up systems, which we term TPV sub-systems.

We note that our review is primarily based on conversion efficiency as the figure of merit for evaluating state-of-the-art TPV technologies. While commercial application of TPV generators will ultimately rely on cost metrics, assessment of system costs can be challenging given the technology's current readiness level. Conversion efficiency, which is directly related to cost-sensitive metrics,⁵ is better suited for identifying promising component materials for continued development. Furthermore, while the total system efficiency of TPV generators captures upstream primary energy conversion and heat transfer losses, TPV-based energy systems are fundamentally limited by conversion of heat into thermal radiation, and radiation into electricity. Other factors directly impacting total system efficiency depend on the heat source (e.g., solar thermal efficiency, burner efficiency, adiabatic efficiency) and can be derived separately from the metrics used here.

Although total system efficiencies of solar-,^{8,10,14,22} chemical-,^{23,24} and nuclear-sourced²⁵ TPV generators are relatively low (4-8%) compared to well-established energy systems such as natural gas combined-cycle power plants, TPVs are generally too technologically immature to be compared at that level. Substantial research efforts and resources are needed to develop TPV components at the necessary scale for prototypical generators to approach the potential efficiencies set by the emitter and cell materials. These challenges should not impede progress in the development of high-performance cell and emitters. In this review, we therefore emphasize the performance of emitter-cell pairs and TPV sub-systems, as defined in the following sections.

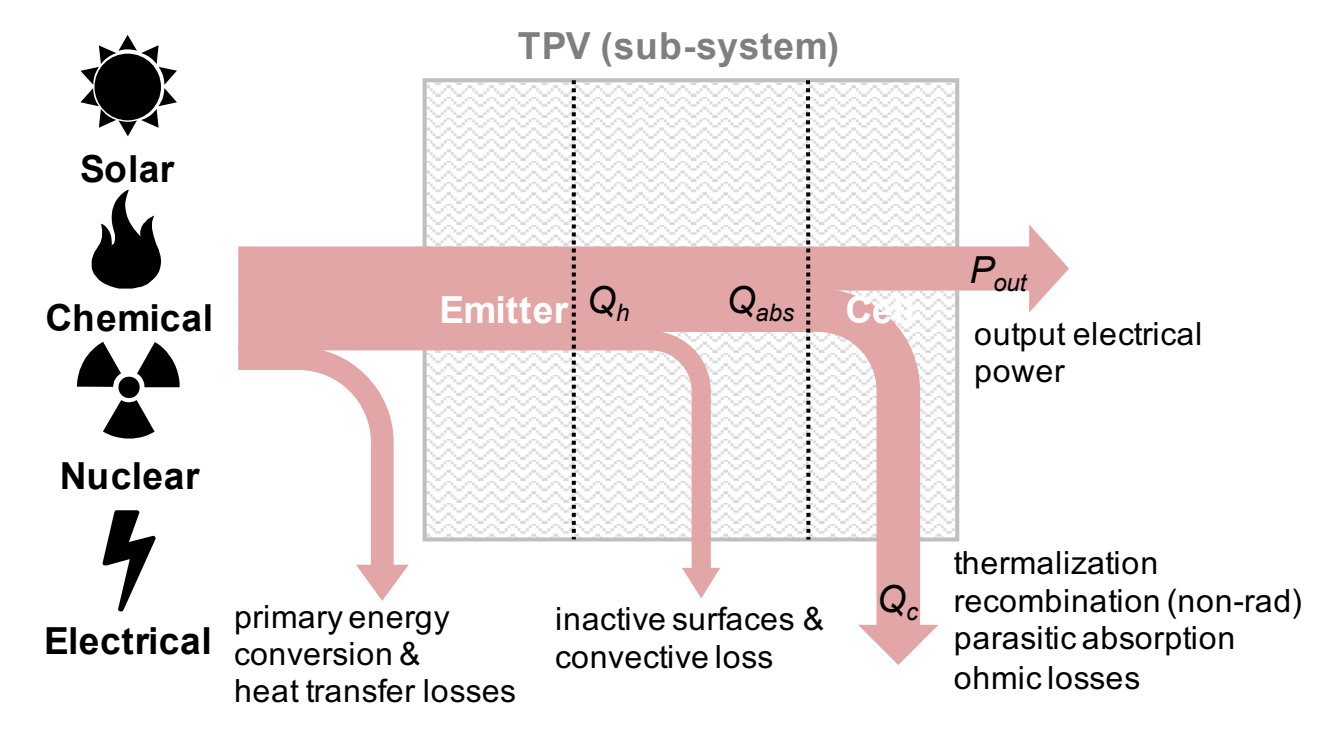


Figure 1. Energy transport and conversion in a thermophotovoltaic generator. Upstream conversion of an energy source heats the thermal emitter, generating radiation that interacts with the cell. Photoexcitation (by in-band radiation) and separation of charge carriers in the cell enables power generation (P_{out}). A portion of incident radiation is reflected by the cell and returned to the emitter (i.e., photon recycling/recuperation). Q_h denotes net energy flow out of the emitter and Q_{abs} denotes radiation absorbed at the cell. Loss pathways within the TPV sub-system include (i) emission to non-current-generating surfaces in the cavity (e.g., edges, contact lines, etc.) and convective loss from the emitter, and (ii) cell inefficiencies, such as thermalization, non-radiative recombination, out-of-band absorption, and Ohmic losses. Upstream inefficiencies related to conversion of the energy source and heat transfer to the emitter depend on the source and are not attributed to the TPV sub-system in this work.

1. Efficiency definitions and limits

This review considers TPV sub-system efficiency $\eta_{TPV} = P_{out}/Q_h$ and TPV pairwise efficiency $\eta_{pairwise} = P_{out}/Q_{abs}$ as the figures of merit for evaluating state-of-the-art TPV technologies, where P_{out} is the generated electrical power, Q_h is the heat flow out of the emitter surface, and Q_{abs} is the heat absorbed by the cell (Fig. 1). These metrics are appropriate for analysis of various TPV emitter-cell pairs and devices. If a study reports additional upstream losses, 14,22,26 those were decoupled to allow for direct comparison across TPV literature. We note that $\eta_{pairwise}$ is equivalent to η_{TPV} in the case of an ideal, lossless cavity ($Q_{abs} = Q_h$). $\eta_{pairwise}$ has also been termed "radiative heat conversion efficiency" elsewhere. We utilize $\eta_{pairwise}$ to identify promising emitter and cell materials/pairs for further scale up and development because it decouples loss mechanisms inherent to materials from inefficiencies resulting from component integration.

To identify which aspects of current TPV designs and materials are favorable, η_{TPV} is further written in terms of a product of several performance metrics:

$$\eta_{TPV} = \frac{P_{out}}{Q_h} = (SE \cdot IQE)(VF)(FF)(CE)$$
(1a)

$$\eta_{TPV} = \left(\frac{J_{sc}V_g}{Q_{abs}}\right) \left(\frac{V_{oc}}{V_g}\right) \left(\frac{J_{mpp}V_{mpp}}{J_{sc}V_{oc}}\right) \left(\frac{Q_{abs}}{Q_h}\right) \tag{1b}$$

where *SE* is spectral efficiency, *IQE* is internal quantum efficiency, *VF* is voltage factor, *FF* is fill factor, and *CE* is cavity efficiency. Each metric is described analytically in Box 1.

The product of the spectral efficiency SE and the internal quantum efficiency IQE describes the conversion of radiative heat absorbed by the cell Q_{abs} into short-circuit current J_{sc} multiplied by the cell bandgap voltage V_g , as shown in Equation 1b. It is mainly a measure of the quality of spectral management in a TPV. Although it shares similarities to the ultimate efficiency,²⁸ the metric has been modified here to accommodate two-way radiative exchange between the cell and thermal emitter. Box 1 shows how SE accounts for multiple reflections between the emitter and the cell using the effective emissivity of a pair.²⁹ Spectral inefficiencies affecting SE include absorption of out-of-band photons, reflectance of in-band photons, and thermalization of highenergy in-band photons. Efforts to improve SE include the use of selective emitters, cells and filters, which aim to suppress out-of-band emission while enabling transfer of in-band light. While

diminishing returns are expected as a single component approaches ideal suppression of out-of-band radiation, simultaneous use of selective components is practically advantageous, as selective cells may suppress radiative transfer in wavelength ranges poorly managed by the selective emitter, and vice versa. Meanwhile, parasitic absorption of in-band photons (e.g., free carrier absorption) and short diffusion lengths of photogenerated carriers lead to losses in *IQE*.

The voltage factor VF and the fill factor FF are measures of charge carrier management. More specifically, voltage factor is a measure of bandgap utilization, describing the ratio of the open circuit voltage V_{oc} to the bandgap voltage V_g . Fill factor describes the ratio of generated power $P_{out} = J_{mpp}V_{mpp}$ to the product of short-circuit current density J_{sc} and open-circuit voltage V_{oc} . It primarily captures the effects of series and shunt resistance, although cell temperature T_c can play a role as well.

Cavity efficiency, $CE = Q_{abs} / Q_h$, describes the effectiveness of emitter-cell integration and is penalized by imperfect view factor, non-current-generating (i.e., inactive) areas on the cell, such as contact lines, and convective loss from the emitter. It is valuable for identifying problematic scaleup effects, such as parasitic thermal losses, compromises made in component integration, or difficulties fabricating large-area materials while maintaining peak performance.

We evaluate the above performance metrics with respect to their upper bounds, as described in the radiative limit. We note that the radiative limit is not only a function of bandgap, but also depends on the temperatures of the emitter and cell. Hence, we cannot provide a singular limit that applies to all cells with a given bandgap (as is common in solar PV literature). Rather, we provide radiative limit metrics, denoted by "rad" subscripts, specific to select emitter-cell pairs, as calculated from reported E_g , T_h , and T_c using the analytic expressions in Box 1. The upper bound of η_{TPV} is then the product of each performance metric in the radiative limit. Normalized values are calculated as the ratio of experimentally observed values to corresponding limits.

Box 1. Definitions and limits of TPV performance metrics.

	Definition	Radiative limit
SE · IQE ^{a,b}	$\frac{J_{sc}V_g}{Q_{abs}} = \frac{E_g \cdot \int_{E_g}^{\infty} \varepsilon_{eff}(E) \cdot IQE \cdot b(E, T_h) dE}{\int_0^{\infty} \varepsilon_{eff}(E) \cdot E \cdot b(E, T_h) dE}$	$\frac{E_g \cdot \int_{E_g}^{\infty} b(E, T_h) dE}{\int_{E_g}^{\infty} E \cdot b(E, T_h) dE}$
VF°	$rac{V_{oc}}{V_g}$	$\left(\frac{k_B T_c}{q V_g}\right) \cdot \ln \left(\frac{J_{sc}}{J_{0,rad}} + 1\right)$

FF	$rac{J_{mpp} \cdot V_{mpp}}{J_{sc} \cdot V_{oc}}$	$\frac{\left(\frac{V_{mpp}}{V_{th}}\right)^{2}}{\left[1 + \frac{V_{mpp}}{V_{th}} - \exp\left(\frac{-V_{mpp}}{V_{th}}\right)\right] \cdot \left[\frac{V_{mpp}}{V_{th}} + \ln\left(1 + \frac{V_{mpp}}{V_{th}}\right)\right]}$
CE	$rac{Q_{abs}}{Q_h}$	1
$\eta_{pairwise}$	$SE \cdot IQE \cdot VF \cdot FF$	$SE_{rad} \cdot IQE_{rad} \cdot VF_{rad} \cdot FF_{rad}$
η_{TPV}	$SE \cdot IQE \cdot VF \cdot FF \cdot CE$	$SE_{rad} \cdot IQE_{rad} \cdot VF_{rad} \cdot FF_{rad} \cdot CE_{rad}$

E is photon energy, q is the charge of an electron, $V_{th} = \frac{k_B T_c}{q}$ is the thermal voltage, and the "mpp" subscript denotes

the maximum power point voltage (V) and current density (J).

^aEffective emissivity of an emitter-cell pair: $\varepsilon_{eff} = \frac{\varepsilon_e \varepsilon_c}{\varepsilon_e + \varepsilon_c - \varepsilon_e \varepsilon_c}$, where ε_e and ε_c are the emissivity of the emitter and cell, respectively.

^bSpectral photon flux of a black body: $b(E, T) = \frac{2\pi E^2}{c^2 h^3 \left(\exp\left(\frac{E}{k_B T}\right) - 1\right)}$, where c is the speed of light in vacuum, h is Planck's constant, and k_B is Boltzmann's constant.

°Dark current density: $J_0 = J_{SC} \left[\exp \left(\frac{qV_{oC}}{k_B T_c} \right) - 1 \right]^{-1}$

In the radiative limit: $J_{0,rad} = \frac{2 \cdot q}{h^3 \cdot c^2} \pi (n^2 + 1) k_B T_c \left(2k_B^2 T_c^2 + k_B T_c E_g + E_g^2 \right) \exp \left(\frac{-E_g}{k_B T_c} \right)$, where the real part of the refractive index n = 3.6 (0) corresponds to the radiative limit in the absence (presence) of photon recycling. ³⁰

2. Record-efficiency TPV pairs compared to the radiative limit

Here we compare leading emitter-cell pairs to each other and to radiative limits in order to identify favorable features and technology gaps. Our use of the term "leading" refers to a given emitter-cell pair exhibiting the highest $\eta_{pairwise}$ in a group of like pairs, as defined by their shared cell material. We have grouped pairs by cell material since the cell bandgap also corresponds to the desired emitter cutoff energy (E_{cutoff}).

Figure 2 shows the best pairwise efficiencies as reported (Fig. 2a) and normalized by corresponding radiative limit efficiencies (Fig. 2b). We further depict a timeline of historical improvements to leading pairwise efficiencies in Fig. 2c. A summary of key technological advancements enabling improvements to efficiency over time is provided in Appendix A. Normalized, thermodynamic efficiencies are considered for further analysis because test conditions, particularly T_h , vary greatly across the TPV literature (see Appendix B for radiative limit calculations for leading pairs). Hence, comparison of absolute efficiencies provides limited insight into the quality of emitter-cell pair design.

The 2019 demonstration of a thin-film lattice-matched, 0.75 eV InGaAs cell (hereafter LM InGaAs) paired with a ~1480 K graphite emitter represents the highest reported absolute pairwise efficiency (29.1%) for any TPV pair in the literature.³¹ This pair also achieves the highest fraction of its radiative limit efficiency (~49%). Similar absolute efficiency has been reported by Swanson (1980) for a Si cell paired with a 2300K blackbody emitter (29%).³² However, when comparing efficiencies to the radiative limit, the Si-based pair falls short of the LM InGaAs-based pair (43.7% vs. 49%) due to the large difference in emitter temperature.

High pairwise conversion efficiencies, exceeding 20%, have also been reported for lattice-mismatched 0.6 eV InGaAs (hereafter 0.6 eV InGaAs) paired with a 1312K graybody SiC emitter³³ and with a 1328K selective emitter (2D Pt puck array on Al₂O₃/Pt stack).³⁴ Lastly, $\eta_{pairwise}$ above 20% has also been reported for a GaSb cell paired with a 1548K W emitter.²³ These demonstrations also represent some of the highest thermodynamic pairwise efficiencies.

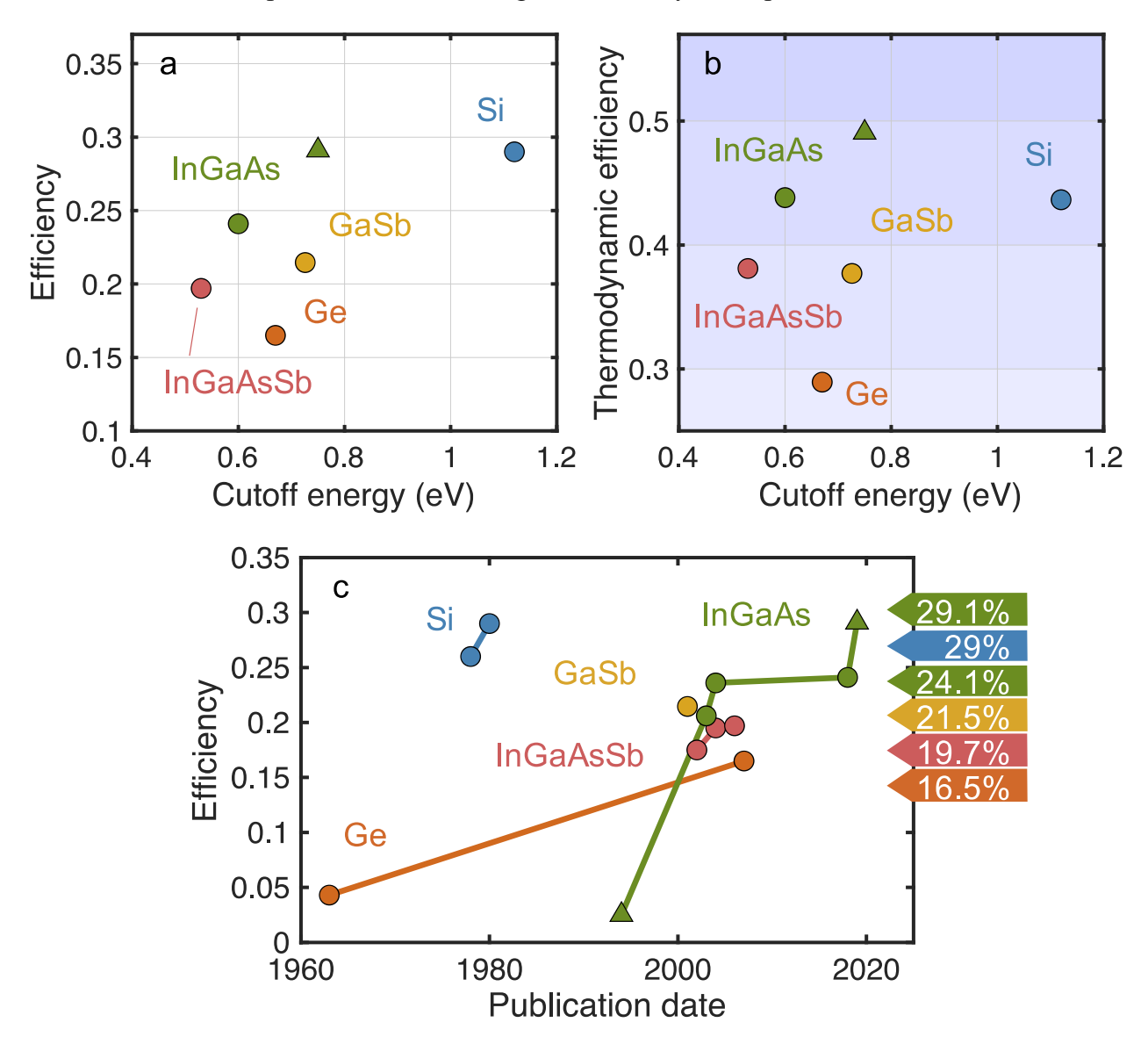


Figure 2. Record pairwise efficiencies spanning cell materials. (a) Absolute efficiencies as reported. (b) Thermodynamic efficiencies, normalized against the radiative limit. (c) Historical

progression of record pairwise efficiencies. Reporting literature: InGaAsSb^{35,99,100}; 0.6 eV InGaAs^{33,34,101}; Ge^{36,102}; GaSb²³; LM InGaAs^{31,42} (triangular markers); Si.^{32,103}

Overall, we observe that leading pairwise efficiencies remain well below their respective radiative limits (< 50%). By contrast, leading solar PV cells have achieved efficiencies exceeding 75% of their corresponding radiative limit. This analysis reveals that TPV technologies remain immature compared to solar PVs, but does not yet offer insights into the shortcomings of leading designs.

To provide a deeper understanding of current limitations, we collected experimental *VF* and *FF* data and calculated *SE·IQE* from reported metrics for leading emitter-cell pairs (Fig. 3, Table 1). Fig. 3a depicts emitter-cell pair performance relative to the radiative limit and compactly decouples contributions according to spectral and charge carrier management. The quality of spectral management is quantified as the ratio of the reported product of *SE* and *IQE* to the corresponding product in the radiative limit, depicted as the vertical axis in Fig. 3a. Similarly, the horizontal axis depicts the corresponding ratio for *VF* and *FF*, representing the quality of charge carrier management.

We observe that the three highest efficiency TPV pairs (with LM InGaAs, Si, and 0.6 eV InGaAs cells) exhibit the best spectral management, approaching ~70% of the radiative limit for *SE·IQE*. This result is consistent with the widely recognized notion that management of the broad spectrum of thermal radiation is critical in TPVs. The cell used for the leading Si-based pair utilizes a SiO₂/Ag back surface reflector (BSR) to achieve ~95% out-of-band reflectance and facilitate the photon recuperation process. Similarly, the leading LM InGaAs-based pair utilizes a cell with a Au BSR. The high out-of-band reflectance (~94%) is enabled by the cell's thin-film architecture. Removal of the InP parent substrate eliminates a parasitic absorption mechanism previously observed for LM InGaAs cells. ⁴² In each case, the cell's high out-of-band reflectance promotes efficient spectral utilization, even under illumination by a broadband emitter. The leading 0.6 eV InGaAs-based pair, on the other hand, relies on a 2D metamaterial selective emitter and a dielectric front surface filter (FSF) to minimize undesired absorption in the cell. The narrower bandgap cell used in this pair is better suited for the emitter temperature, which serves to benefit *SE*. While this strategy appears to offer similar out-of-band suppression to those described above, we cannot make a direct quantitative comparison as cell reflectance properties are not provided. The quality of

spectral management among these leading pairs highlights the importance of spectral efficiency (SE) in achieving high conversion efficiency. Further, we note the common use of out-of-band reflectance (by a BSR or FSF) as a technique to facilitate spectral management among these leading pairs.

In terms of carrier management, the leading LM InGaAs-based pair exhibits the best $VF \cdot FF$, exceeding 70% of the corresponding radiative limit. This is largely attributed to the cell's high V_{oc} , which translates to the highest normalized VF among pairs considered here. While V_{oc} generally increases with illumination intensity, this particular VF is not attributed to differences in illumination, as the leading LM InGaAs-based pair is characterized at $J_{sc} = 0.92$ A cm⁻², which is low relative to other leading pairs. Beyond this consideration, differences in cell growth and resulting material quality may affect the quality of charge carrier management. The leading LM InGaAs and 0.6 eV InGaAs cells were both grown by metal-organic vapor phase epitaxy (MOVPE) on an InP substrate. However, the leading LM InGaAs-based pair exhibits higher normalized VF (0.71) than that of the 0.6 eV InGaAs-based pair (0.63). Notably, it is more challenging to achieve low defect densities in a cell utilizing a buffer layer to overcome lattice mismatch, as is necessary for growth of 0.6 eV InGaAs epitaxial layers on InP.⁴³

We also note that the bandgap/cutoff energy of leading pairs does not maximize SE, given their respective T_h and level of selectivity (see Fig. 4a,d and Fig. C1). In general, the bandgap exceeds the value that optimizes SE. For example, Woolf, $et\ al$. utilize a 0.6 eV InGaAs cell in tandem with an emitter at $T_h = 1328$ K, whereas $E_g \approx 0.5$ eV would maximize SE at these operating conditions. While lower E_g is desirable for improving SE, detrimental side effects on carrier management were likely considered in the design of leading pairs. In particular, lower E_g increases the portion of in-band radiation, thereby increasing J_{sc} . At high J_{sc} , Ohmic losses can reduce FF, which may outweigh the benefit to SE. Further, as bandgap narrows, thermal generation produces a larger intrinsic carrier concentration, n_i , increasing proportional loss to recombination and decreasing VF. Therefore, optimal SE may not correspond to maximized $\eta_{pairwise}$ (see Appendix C for performance metric calculations as a function of E_g).

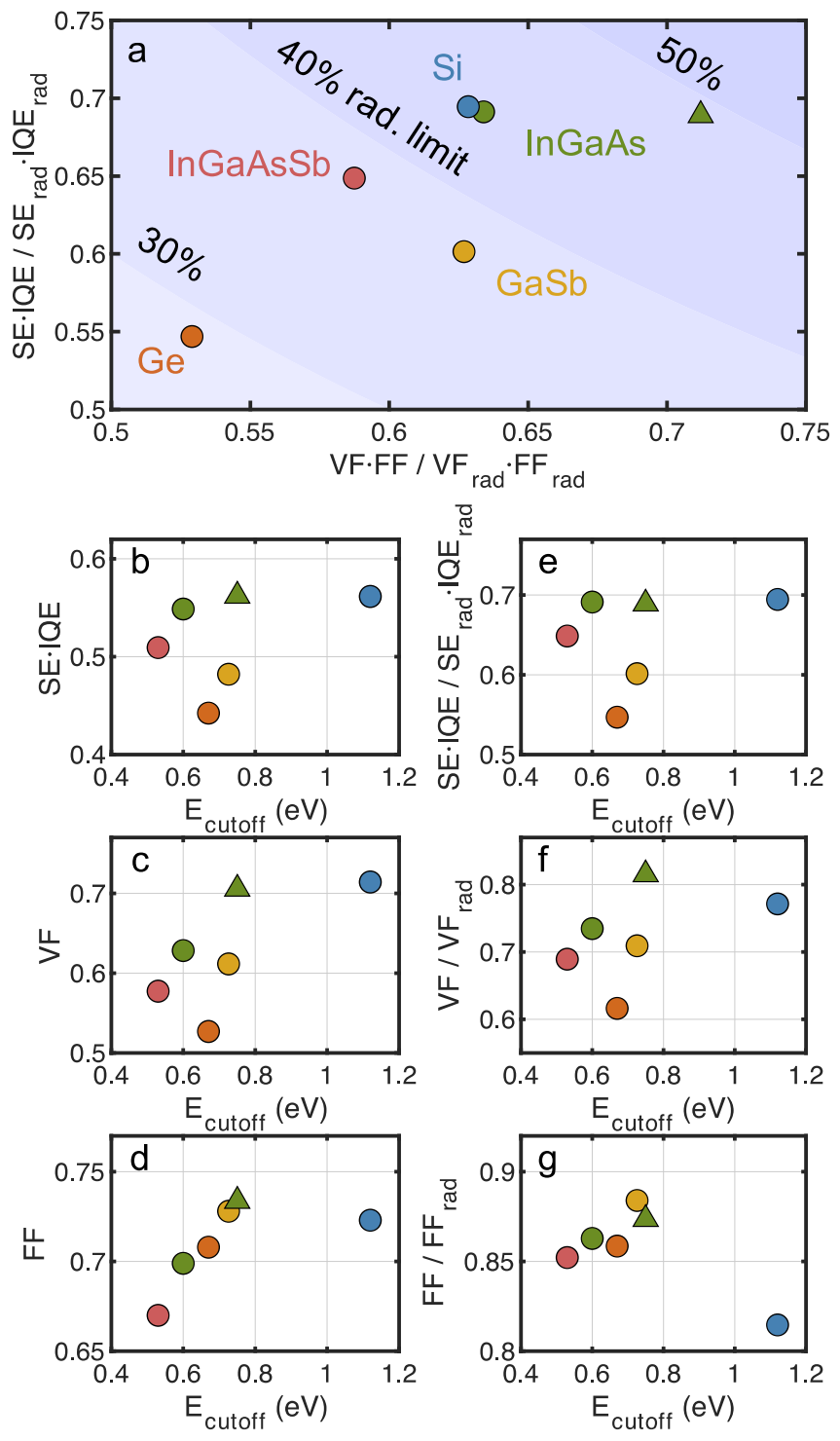


Figure 3. Characteristics and limitations of leading TPV pairs. (a) The product of *SE* and *IQE* describes the quality of spectral management. *VF* and *FF* characterize the effectiveness of charge carrier management. Normalization to corresponding values in the radiative limit provides a basis for identifying target metrics for improvement. (b-d) Reported, absolute performance metrics. (e-g) Performance metrics, normalized to corresponding values in the radiative limit. Reporting literature: InGaAsSb³⁵; 0.6 eV InGaAs³⁴; Ge³⁶; GaSb²³; LM InGaAs³¹ (triangular markers); Si.³²

Table 1. Leading TPV emitter-cell pairs by cell material class (Figs. 2, 3, & 5).

Cell	E _g [eV]	<i>T_c</i> [K] ^a	Emitter	<i>T_h</i> [K]	J _{sc} [A cm ⁻²]	<i>V</i> _{oc} [V]	J_{θ} [A cm ⁻²]	SE·IQE ^b	VF	FF	η _{pairwise} [%]	$oldsymbol{\eta_{pairwise,rad}}$ [%]	Ref
InGaAsSb	0.53	300	SiC plate	1223	2.9	0.31	2.36x10 ⁻⁵	0.51	0.58	0.67	19.7	51.7	35
0.6 eV InGaAs	0.6	-	Pt array on Al ₂ O ₃ /Pt	1328	0.72	0.38	2.35x10 ⁻⁷	0.55	0.63	0.70	24.1	55.0	34
Ge	0.67	-	Micro- structured W	1373	1.65	0.35	1.40x10 ⁻⁶	0.44	0.53	0.71	16.5	57.0	36
GaSb ^c	0.73	323	W foil with ARC	1548	3.52	0.45	3.73x10 ⁻⁷	0.48	0.62	0.73	21.5	56.9	23
LM InGaAs	0.75	293	Graphite $(\varepsilon \approx 0.9)$	1480	0.92	0.53	7.24x10 ⁻¹⁰	0.56	0.71	0.73	29.1	59.3	31
Si	1.12	-	Presumed blackbody	2300	8.76	0.8	1.52x10 ⁻¹³	0.56	0.71	0.72	29.0	66.4	32

^aIn cases where T_c has been omitted in the relevant publication, $T_c = 293$ K has been assumed for relevant calculations.

3. Spectral management

In this section, we decouple the effects of emitter and cell properties to survey emerging component-wise approaches for TPV spectral management. Prior reports have sought to describe emitter-specific spectral efficiency as the ratio of in-band power to total emitted power, 44 and therefore defined cell efficiency in terms of the conversion of in-band power. This formulation, however, neglects the cell's role in modifying the spectrum of Q_{abs} , and cannot be easily generalized to pairs with reflective cells. To provide a more complete description of component-wise contributions to spectral management, we investigate the properties of a single component by considering its spectral efficiency when paired with a theoretical blackbody (non-selective) counterpart. This metric is termed "individual SE".

 $^{{}^{}b}SE \cdot IQE$ is calculated from reported $\eta_{pairwise}$, VF, and FF.

^cIn the case of GaSb, only simulated *VF* and *FF* are reported.

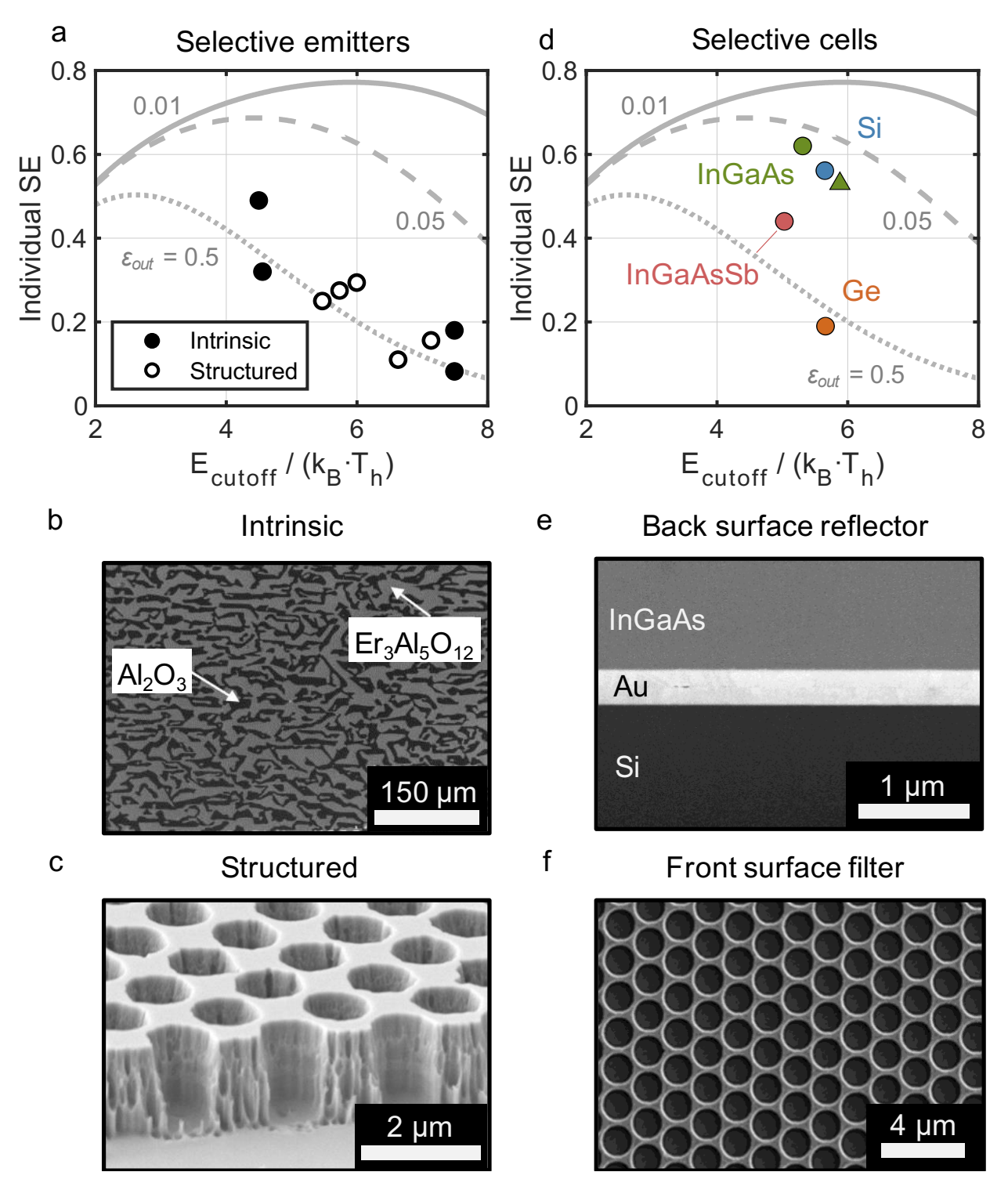


Figure 4. Component-wise spectral control strategies. Individual spectral efficiencies of (a) selective emitters and (d) selectively absorptive cells. Experimental values are compared to SE curves for various out-of-band emissivities with ideal in-band absorption ($\varepsilon_{in} = 1$). Examples of spectral control structures: (b) Al₂O₃/Er₃Al₅O₁₂ eutectic ceramic, ⁴⁵ (c) 2D W cavity array, ⁴⁶ (e) thin-film LM InGaAs with Au BSR, ⁴⁷ (f) 2D photonic crystal front-surface filter on a GaSb cell. ⁴⁸

3.1 Selective Emitters

Selective thermal emitters are designed to preferentially emit in-band radiation, while simultaneously suppressing out-of-band emission. We narrow the scope of surveyed emitters to (i) those that have been heat treated at or above 1023 K (750°C) for over 1 hour and (ii) whose optical properties were characterized at or above 1023 K (750°C). Appendix D contains emitters characterized near room temperature. The first criterion was selected because, beyond degraded spectral performance, if an emitter is unstable, material may evaporate and subsequently deposit onto the cell. Hence, long-term thermal stability is important for the reduction of operation and maintenance costs. While one hour of thermal aging does not sufficiently demonstrate the degree of stability required for practical application, this criterion is appropriate given the current technology readiness level of emerging emitters. In some cases, one hour of aging at temperatures in excess of 1000° C can reveal major instabilities. The second criterion is required because emissivity is temperature dependent. Measurement of thermal emissivity near room temperature has been shown to significantly underestimate the actual thermal emissivity at high temperatures. We therefore calculate individual *SE* based on reported spectra measured at high temperatures (T_h in Table 2).

Fig. 4a shows the individual SE of various emitters that meet the above criteria, compared to analytical curves for perfect, in-band absorption ($\varepsilon_{in} = 1$) and a range of out-of-band suppression. We show the theoretical curves in this way because decreasing out-of-band emission/absorption has a greater effect on SE than increasing in-band emission/absorption due to the relative power in each band. In this analysis, we have categorized the emitters according to two groups: (i) intrinsically selective materials such as transition metal and rare earth oxides (Fig. 4b) and (ii) structurally tunable thermal emitters exhibiting geometry-dependent spectral properties (Fig. 4c). Tunable emitters typically leverage periodic architectures with one-dimensional (i.e., alternating stacks), two-dimensional (i.e., cavity or pillar arrays), or three-dimensional (i.e., inverse opal networks) periodicity at a length-scale on the order of the wavelength of interest.⁵¹ Individual SE calculations generally follow theoretical curves for the corresponding ε_{out} ; deviation from these curves is the result of non-ideal in-band absorption ($\varepsilon_{in} < 1$).

In terms of the best spectral efficiency exhibited among intrinsically selective materials, a MgO emitter with NiO loading⁵² achieves a notable 49% spectral efficiency. Introducing

transition-metal dopant ions within a low emissivity MgO host lattice leads to selective emission due intra-atomic electronic transitions. These transitions are determined by the electronic configuration of the dopant ions and interactions with the lattice of the host oxide. Dopant concentrations of 1–2 mol% appear to be optimal because of a tradeoff between nearest neighbor interactions and peak spectral density. Our survey also shows that intrinsic emitters generally exhibit better thermal stability. Despite these noteworthy results, relatively few papers have explored the use of transition-metal dopants in TPV emitters. As such, their ability to tailor emission properties to match the bandgap of a cell remains limited.

Alternatively, structured emitters offer improved control over the emission cutoff energy. The leading structured thermal emitter is a W 2D photonic crystal emitter with a cavity array geometry that exhibits 29.4% individual SE. Enhanced in-band emission occurs by coupling into resonant electromagnetic cavity modes, while emission is suppressed below the cavity resonant frequency. The resonant frequency, and therefore cutoff energy, of the emitter may be tuned by varying cavity diameter and depth. Further, the sharpness of the transition is a result of geometrical uniformity. Another high-performance structured emitter with individual SE = 27.5% utilizes a similar structure, consisting of a Ta-W alloy with a HfO₂ coating. The considerable difference in individual SE between the best intrinsic and leading structured emitters is largely due to the lower demonstrated temperatures of structured emitters.

Other structured emitters, characterized near room temperature, exhibit promising spectral properties (see Appendix D). For example, a HfO₂/Mo/HfO₂ emitter leverages its ultrathin Mo absorber layer (much thinner than the wavelength) and a Fabry-Perot cavity created between the top interface and the bottom reflector to achieve coherent perfect absorption at a wavelength near the cell's bandgap.⁵⁴ Similar structures, where a refractory metal such as W is sandwiched between dielectrics, have also exhibited comparable spectral efficiencies based on room temperature emissivity measurements.^{55,56} However, it is unclear if these promising properties will translate to high performance at operating temperatures. Future studies should thus strive to report data at high temperatures.

The primary failure mechanisms of structured emitters appear to be oxidation of the metal layers and growth of dielectric grains, both of which are activated by high temperatures.⁵⁵ However, the kinetics of these mechanisms can be slowed by operating under moderate vacuum and below the grain growth temperature threshold.

One promising way to stabilize emitters appears to be the use of transparent refractory coatings. Nearly all tunable, selective emitters that meet our heat treatment criteria integrate a refractory metal / metal oxide component. Low-defect refractory coatings enhance thermal stability by impeding surface reactions and inhibiting diffusion. Fig. 7 Prior studies have identified HfO2 as a leading candidate among refractory materials for improved stability. Integration of refractory materials may help to improve the thermal stability of emitters designed solely for high selectivity at room temperature. While tunable, selective emitters may rely on nano- and micropatterned designs to achieve selectivity, the resulting void space in 2D and 3D geometries leave materials susceptible to thermal degradation. One proposed strategy for improved stability in 2D and 3D structured emitters is to fill void space with an additional material, thereby achieving bulk planar geometry while maintaining the necessary patterning for selectivity. Decreased structural curvature through modified periodicity and smoother geometrical transitions has also been shown to alleviate thermal degradation of cavities.

A widely proposed plan to protect the cell from material deposition under an unstable emitter is the use of an intermediate glass cover or a gas purge.⁶² However, out-of-band absorption in a deposition shield may limit the effectiveness of cell-side spectral control, such that the pair relies on the emitter's optical properties for achieving high *SE*. Furthermore, operation at elevated radiative power densities may be required to decrease the relative effect of convective losses associated with a gas purge/curtain.

Overall, it appears that significant improvements in spectral efficiencies are possible through additional materials development. Furthermore, high-temperature aging data for selective emitters is lacking. Longer thermal aging studies are necessary to identify failure mechanisms and suitable operating conditions.

Table 2. Selective thermal emitters that were heat treated above 1023K for at least 1 hour and with emissivity measured at temperatures >1023K (Fig. 4a.). Emissivity data extracted from relevant

publications is available for download (see SI).

Emitter description		E _{cutoff} [eV]	Measurement Temperature T_h^a [K]	E_{cutoff} / k_BT_h	€ out b	€in ^b	Ind. SE ^c	E range [eV] / BB fractiond	Heat treatment conditions	Ref
	MgO with 2wt% NiO loading	0.65	1677	4.5	0.18	0.71	0.49	0.14-1.14 / 93%	1793K, duration omitted	52
Intrinsic	Al ₂ O ₃ /Er ₃ Al ₅ O ₁₂ eutectic	0.73	1850	4.58	0.27	0.43	0.32	0.62-1.4 / 40%	In air at 1973K for 1000 hr	45
	Yb₂O₃ foam	1.12	1735	7.49	0.29	0.54	0.082	0.075-1.6 / 99%	1750K for 200 cycles, duration omitted	63
	Yb ₂ O ₃ mantle	1.12	1735	7.49	0.14	0.62	0.18	0.024-1.6 / 99%	1750K for 200 cycles, duration omitted	63
	Pt array on Al ₂ O ₃ /Pt	0.6	1273	5.47	0.47	0.93	0.25	0.25-1.4 / 76%	In Ar at 1273K for 2 hr	34
	W 2D cavity (D = 1.1µm) array	0.62	1200	6.00	0.25	0.86	0.294	0.16-1.3 / 90%	Under vacuum at 1200K for 10 hrs	46
Structured	Ta 2D cavity array with HfO ₂ coating	0.62	1255	5.73	0.34	0.89	0.275	0.41-0.89 / 40%	Under vacuum at 1273K for 1 hr / 1173K for 144 hr	53
	HfO ₂ coated W inverse colloidal 3D PhC	0.67	1173	6.63	0.62	0.91	0.11	0.25-0.98 / 71%	In Ar at 1673K for 1	49
	W 2D cavity (D = 900nm) array	0.73	1186	7.14	0.30	0.94	0.156	0.16-1.3 / 90%	Under vacuum at 1200K for 10 hrs	46

 $^{{}^{}a}T_{h}$ refers to the measurement temperature at which spectral emissivity was characterized.

3.2 Selective cells

As introduced above, an alternative approach for spectral control is reflection of out-of-band radiation back to the emitter using a selectively absorptive cell. This is typically achieved through use of a back-surface reflector (BSR) (Fig. 4e) and/or a front-surface filter (FSF) (Fig. 4f). One practical advantage of this spectral control strategy is that pairs are not constrained by the requirement of material stability at high operating temperature. This may enable the design and use of a richer set of photonic architectures. We note, however, that this approach is more sensitive

^bWeighted average out-of-band emissivity (ε_{out}) and in-band emissivity (ε_{in}) have been calculated using spectral properties collected from graphical data. Error may have resulted from the data extraction process.

^cIndividual SE calculations are based on spectral emissivity data. We extrapolate average emissivity values by band to the limits of integration to account for truncated data. Therefore, our calculated values may deviate from those values reported elsewhere. We note the reported spectral range as a measure of certainty for individual SE calculations. ^dThe reported spectral range used to calculate SE and the fraction of the emissive power at the given T_h captured by this range are provided.

to cavity non-idealities when compared to selective emitters, since well-insulated cavities are required to return reflected radiation back to the emitter.^{64,65}

Fig. 4d and Table 3 show the individual spectral efficiencies of representative TPV cells, given a blackbody emitter at the temperature indicated by the relevant publications. We observe that a 0.6 eV InGaAs cell developed by Wernsman, *et al.* has the highest individual spectral efficiency to date (62%).³³ We note, however, that this is not the same cell as that of the leading 0.6 eV InGaAs-based pair. This advance was enabled by utilization of a BSR and FSF to achieve low parasitic, out-of-band absorption and operation at a high emitter temperature, well-suited for the given bandgap.

Notably, other leading designs have performed similarly well out-of-band. Removal of the growth substrate from epitaxial cells has helped to improve *SE* by eliminating parasitic absorption associated with substrate counter-doping or buffer layers.^{31,66} For example, Omair, et al. reported 94% out-of-band reflectance, enabled in part by removing the InP parent substrate.³¹

Beyond simple semiconductor-on-metal architectures, use of dielectric spacers at the back of the active layer has been shown to improve out-of-band reflectance for Ge, LM InGaAs, and InGaAsSb cells. ^{36,47,66,67} Fernandez, *et al.* report a Ge cell with a SiO₂ / Al BSR that exhibits a 5% absolute out-of-band reflectance improvement compared to the same cell with Al alone. ³⁶ Further, Burger, *et al.* report 96% out-of-band reflectance for a LM InGaAs film with a MgF₂ / Au BSR, exceeding that of any cell surveyed here. ⁴⁷

Furthermore, our survey finds that there is room for significant improvements to in-band absorption in many TPV cells. Specifically, *SE* remains unoptimized for non-ideal in-band absorption. For example, the cell used in the leading LM InGaAs-based pair does not exhibit the highest *SE* mainly due to unoptimized in-band absorption.^{31,32} Deposition of an ARC or surface texturing can improve in-band absorption, *SE*, and output power. For example, we estimate that the individual *SE* of the LM InGaAs cell in the record-efficiency pair³¹ would be improved by 7% absolute in the case of perfect in-band absorption. However, unintentional out-of-band absorption resulting from these treatments must be minimized to observe this benefit in practice.

Spectral utilization may also be improved through integration of additional absorbers. TPVs utilizing tandem cells may theoretically surpass the radiative limit *SE* defined above for a single-junction cell. The equation provided in Box 1 for calculating *SE* can be easily extended to

multiple absorbers by splitting up the numerator to account for multiple bandgaps. Development of TPV pairs with tandem cells has been limited,^{68–72} but theoretical studies are promising.⁷³

Table 3. Selectively absorptive cells (Fig. 4d). Emissivity data extracted from relevant publication is available for download (see SI).

Material	E_g [eV]	T _h [K]	E_g/k_BT_h	€ _{out} a	€in ^a	Individual SE ^b	E range [eV] / BB fraction ^c	Ref
InGaAsSb	0.53	1273	4.83	0.24	0.95	0.44	0.31–1.24 / 64%	66
0.6 eV InGaAs	0.6	1312	5.31	0.06	0.76	0.62	0.06–1.48 / 99%	33
Ge	0.67	1373	5.66	0.56	0.80	0.18	0.50–4.94 / 37%	36
LM InGaAs	0.75	1480	5.88	0.06	0.68	0.53	0.08–0.99 / 95%	31
Si ^d	1.12	2300	5.65	0.05	0.55	0.56	-	32

^aWeighted average ε_{out} and ε_{in} have been calculated using spectral properties collected from graphical data. Error may have resulted from the data extraction process.

4. Charge carrier management

Once charges are photogenerated, cells must efficiently collect those charges while maximizing output voltage. Here, we analyze charge carrier management based on effective dark current density, J_0 . To this end, we have calculated J_0 for leading TPV pairs given reported V_{oc} , J_{sc} , and T_c , by assuming an ideality factor, n, of 1 and neglecting shunt losses, using the ideal diode equation:

$$V_{oc} = \frac{k_B T_c}{q} \ln \left(\frac{J_{sc}}{J_0} + 1 \right) \tag{2}$$

Whereas voltage factors are heavily dependent on testing conditions (V_{oc} increases logarithmically with illumination intensity), J_0 offers a more objective metric; it normalizes for the effects of variable illumination and omits the effects of Ohmic loss.

 J_0 values for leading TPV cells are compared to the theoretical minimum with and without photon recycling (Fig. 5). In either case, dark current is expected to decrease with increasing bandgap, as the recombination rates scale with the intrinsic carrier concentration.

^bIndividual SE calculations are based on spectral emissivity data. We extrapolate average emissivity values by band to the limits of integration to account for truncated data. Therefore, our calculated values may deviate from those values reported elsewhere. We note the reported spectral range as a measure of certainty for individual SE calculations. ^cThe reported spectral range used to calculate SE and the fraction of the emissive power at the given T_h captured by this range are provided.

^dIn the case of Si, only ε_{out} is reported. We have supplemented this data with an estimate of ε_{in} based on optical simulation of the reported structure.xs

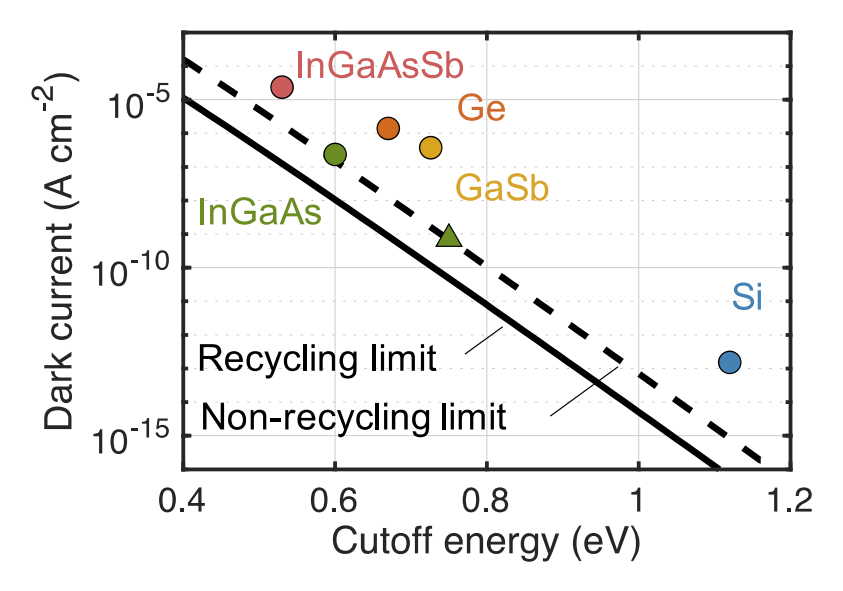


Figure 5. Effective dark current density of leading TPV cells. Radiative limit dark current density with (solid curve) and without (dashed curve) internal photon recycling. Reporting literature: InGaAsSb³⁵; 0.6 eV InGaAs³⁴; Ge³⁶; GaSb²³; LM InGaAs³¹ (triangular marker); Si.³²

We observe that leading pairs with InGaAs cells of both compositions (0.6 eV and LM) exhibit low dark current densities, approaching the non-recycling radiative limit. Thin, crystalline materials, such as these leading InGaAs cells, benefit from high quality growth, limiting defect-mediated carrier recombination. The thin-film geometry can also enhance internal recycling of luminescent photons, further reducing net recombination.^{74–78}

In contrast, GaSb cells exhibit dark current densities nearly two orders of magnitude greater than the non-recycling radiative limit. Prior studies have primarily attributed losses in GaSb to defect-mediated recombination.⁷⁹ Development of doping techniques in GaSb without introducing recombination centers is an ongoing area of research.^{80,81}

Poor dark current among other cell materials considered here may further be the result of technological immaturity. While Si- and Ge-containing cells have witnessed remarkable strides in solar PV applications, development of Si and Ge cells for TPV systems has been limited. Notably, leading Si solar PV cells^{38,39} have ten-fold lower dark current densities than the Si cell in the leading TPV pair.³² Although they face unique challenges, it appears that TPV cells stand to benefit significantly from advances in semiconductor growth and manufacturing to bridge the gap with leading solar cells in terms of charge carrier management.

Our survey reveals that the following design considerations may generally improve carrier management:

- (i) Minimizing series resistance. Whereas Ohmic losses in leading solar PV configurations are effectively negligible, $^{38-40}$ TPV pairs are prone to Ohmic losses, which adversely affect fill factor, since they scale quadratically with current density ($P_{Ohmic loss} = R_s \cdot J_{MPP}^2$). For example, the LM InGaAs cell in the leading pair exhibits R_s of 0.044 Ω cm², resulting in an 8% loss in power output. Given that high power density could be a major advantage for TPV generators, in terms of cost per power (\$/W), alleviating Ohmic losses for high power systems is essential for enabling practical implementation. Lowering series resistance to acceptable levels may require further development and optimization of transparent lateral conduction layers, low interfacial resistance contacts, and metal grids. These considerations are also critical for near-field TPV configurations because of their enhanced power density. $^{82-88}$
- (ii) Thermal management at the cell. Elevated cell temperature results in increased dark current, decreased V_{oc} , and degraded $\eta_{pairwise}$. For example, Wernsman, et al. observe a 43 mV drop in V_{oc} when a 0.6 eV InGaAs cell is heated from 24 to 64 °C, resulting in a 3.6% absolute drop in $\eta_{pairwise}$ under constant illumination.³³ While passive techniques for heat dissipation are attractive, Blandre, et al. show that active cooling techniques may be necessary to meet cooling demands at high power densities.⁸⁹ Though emitter-cell pairs typically require active cooling to maintain cell temperature during characterization at high power densities, $\eta_{pairwise}$ is not penalized by this power consumption. As materials transition to prototypes, power consumed for circulating coolant may reduce overall efficiency, but this effect is expected to be small (<5%) with state-of-the-art thermal management systems.^{90–92}
- (iii) Enhancing internal photon recycling. High back-surface reflectance near the band-edge has been shown to produce V_{oc} gains in high-quality solar cells. ^{74,75,77,78} This effect has yet to be demonstrated in TPV pairs, as radiative recombination is not sufficiently dominant. ³¹ Nevertheless, recent cell-side spectral engineering efforts (discussed in the previous section) are synergistic with this goal. ^{31,47}

(iv) Multi-junction cells. Beyond the potential for enhanced SE, multi-junction cells can enhance V_{oc} and lower J_{sc} compared to single-junction cells. This approach reduces Ohmic losses, which scale quadratically with photocurrent. Ohmic losses are considerably more important for TPV generators compared to their solar counterparts.

5. Toward practical implementation

Major improvements in efficiency measured under idealized conditions are necessary, but not sufficient, for widespread adoption of TPV technology. The performance of emitter-cell pairs needs to translate to prototypes and ultimately generators. This has been an emphasis of many TPV efforts since the early work of Swanson, as discussed in Appendix A. In particular, significant advancements were made toward practical implementation of TPV materials by improving emitter stability, on one hand, and developing quality narrow-bandgap cells that require lower heat source temperatures, on the other. However, more affordable manufacturing technologies are needed for large-scale cell production. Here, we consider the performance of leading TPV sub-systems and discuss approaches for improving practical performance and lowering modular costs.

5.1 Analysis of TPV sub-system efficiencies

We consider TPV sub-system efficiency η_{TPV} as an intermediate performance metric for transition from emitter-cell pairs to prototypes, which captures losses related to imperfect component integration, such as absorption by inactive regions of the cell, non-ideal view factors, and convective loss from the emitter.

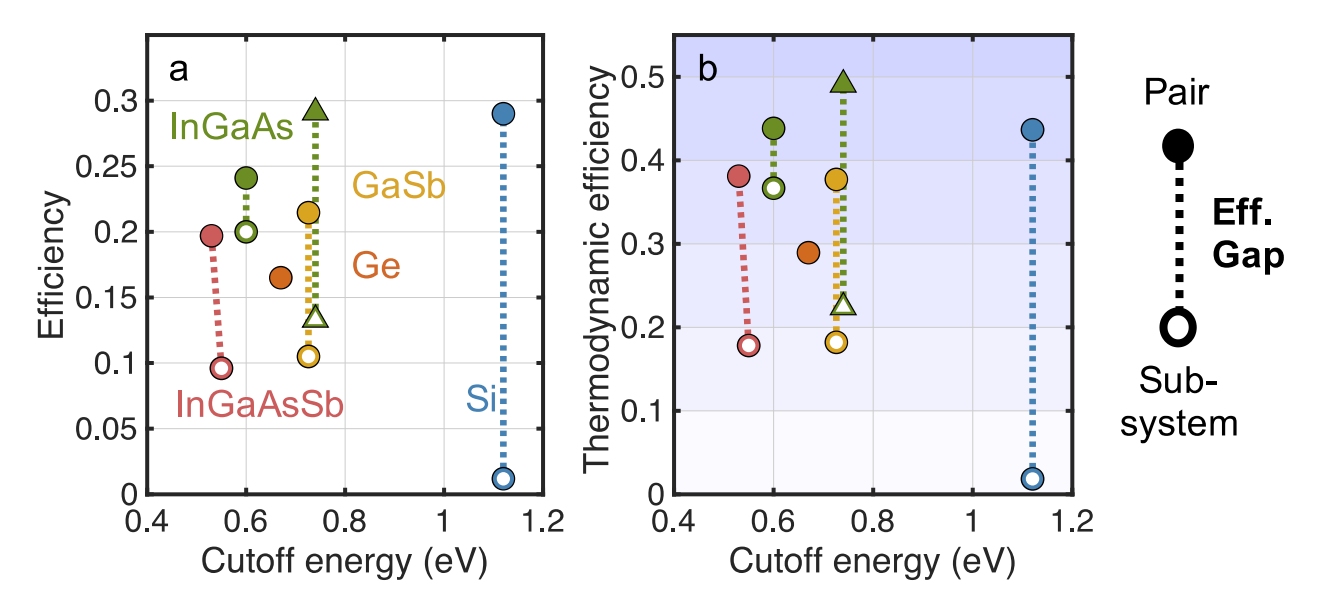


Figure 6. Gaps between pairwise and TPV sub-system efficiencies. Leading pairwise cell efficiencies compared to record sub-system efficiencies. Reporting literature: InGaAsSb^{14,35}; 0.6 eV InGaAs^{34,93}; Ge³⁶; GaSb^{22,23}; LM InGaAs^{26,31} (triangular marker); Si.^{32,94}

Like our survey of emitter-cell pairs, we have identified reports of record-high η_{TPV} among groups by cell material. For 0.6 eV InGaAs- and Si-based sub-systems, η_{TPV} has been measured directly. For InGaAsSb-, GaSb-, and LM InGaAs-based sub-systems, it was deduced from simulated loss breakdowns. For all cases, we observe a notable efficiency gap between leading TPV emitter-cell pairs and leading TPV sub-systems as shown in Fig. 6a (see Appendix E for full dataset). We note that leading TPV sub-systems do not necessarily make use of leading emitter-cell materials considered previously. Therefore, gaps between $\eta_{pairwise}$ and η_{TPV} should not be fully attributed to CE. Overall, we observe that sub-systems with wider bandgap cells (e.g., Si) appear to be more susceptible to these issues. To account for different testing conditions, which could be a confounding variable, we further normalize sub-system η_{TPV} with respect to the radiative limit to account for variable T_h and other factors. However, Fig. 6b shows that the observed gap persists even when comparing thermodynamic efficiencies. To help rationalize the performance gap, we consider the effects of imperfect component integration and scale-up.

Each leading TPV sub-system utilizes a vacuum environment to ensure emitter stability and eliminate convective heat transfer losses. Therefore, the cavity efficiencies of these TPV sub-systems are primarily dependent on their geometrical design, including the view factor between the cell and emitter. Consider, for example, the case of 0.6 eV InGaAs. The highest reported η_{TPV}

for a 0.6 eV InGaAs sub-system is 20%,²⁵ short of the 23.6% pairwise efficiency reported for the same cell under a lamp.³³ In a related report, Crowley, *et al.* attribute this gap to imperfect cavity efficiency, non-uniform cell illumination and inefficiencies related to cell interconnections.⁹³ This sub-system relies on a selective cell to achieve spectral control, and is therefore more susceptible to cavity losses. These loss pathways are common among other sub-systems as well. In the case of GaSb, Bhatt *et al.* report a view factor of 0.85 and attribute this high cavity loss to the small area of the cell relative to the emitter.²² Nonetheless, many of the sub-system heat losses that severely restrict efficiency can be minimized as leading emitter-cell pairs reach the kW-scale.¹⁴

In addition to cavity imperfections, it appears that material supply/scaling issues may also be a factor in some of the observed performance gaps. Both the leading LM InGaAs- and InGaAsSb-based sub-systems have well-designed cavities with view factors of 0.97 and 0.96, respectively. Thus, the drop-off in performance is likely because the LM InGaAs and InGaAsSb cells used in the sub-system did not perform as well as the champion cells.

As TPVs transition toward commercialization, it will become increasingly necessary to address cavity inefficiencies and other scaling issues. One prior study has proposed several design strategies for reducing system sensitivity to cavity losses.⁶⁴ For example, increasing spectral overlap by increasing the ratio of the emitter temperature to the bandgap is expected to make TPV sub-systems less susceptible to such losses. Multi-junction designs, especially, offer a practical means of increasing spectral overlap, lowering Ohmic losses, and improving resistance to cavity inefficiencies. Further, utilization of a selective emitter, even in tandem with a selectively absorptive cell, can reduce sensitivity to parasitic optical loss.

5.2 Opportunities in manufacturing and modular costs

Given current efficiencies and module costs, TPVs remain prohibitively expensive for widespread commercialization. One promising pathway to reduced cost (\$/W) is leveraging high power densities, characteristic of local thermal emission. In theory, high power densities represent one of the technology's greatest assets. In practice, however, Ohmic losses at high current densities can inhibit efficient conversion under high-intensity illumination. Utilization of a MIM architecture reduces individual cell area and therefore, enables low current operation that can alleviate the stringent series resistance requirements of TPV configurations. However, small cells may reduce

cavity efficiency and complicate scale up. Accordingly, efficient operation at high power densities (>3 W cm⁻²) remains a challenging problem that needs to be addressed.

A complimentary approach to lower costs is to grow multiple cells from a single growth substrate. Crystalline III-V substrates persist as the largest single cost of TPV modules. Recovery of a substrate after growth and subsequent reuse can therefore reduce module costs considerably. This approach requires non-destructive liftoff techniques to enable substrate reuse. Promise of substrate reuse, this technique has not been demonstrated for cells in TPV systems. Nevertheless, this manufacturing development appears to be important for commercialization and process sustainability.

TPV module costs stand to benefit from production at a higher volume than current lab-scale manufacturing. Notably, this may require utilization of TPVs in high-volume applications, such as grid-scale thermal energy storage or residential co-generation. Alternatively, it may be necessary for cell fabrication techniques to make use of more mature technologies already in use for production of solar PV or telecommunication components. As development of high-quality Si cells for solar PV application benefitted from advances in integrated circuit technology, concurrent development of other materials for separate applications may expedite their deployment in TPV systems. For example, LM InGaAs and Ge photodiodes are commonly used for optical detection in the near-IR. Further, Ge and various InGaAsSb and InGaAs alloys are common sub-cell materials in multi-junction solar PV technologies. Ongoing research efforts in these areas may benefit the performance and cost metrics of corresponding cell materials in TPV pairs.

6. Discussion

Our review identifies major opportunities for TPV research by comparing leading emitter-cell pairs and sub-systems, spanning a wide range of cell materials (0.5-1.1 eV), to thermodynamic limits. In the near term, it appears that TPV pairs can benefit from certain designs that have advanced the performance of solar cells. For example, design choices that have enhanced internal recycling of luminescent photons, such as high back-surface reflectance, can also enable recycling of low energy photons – a key factor in TPV efficiency. However, TPV generators are faced with unique challenges such as thermal stability of the emitter, tension between cost per power and Ohmic losses associated with high current densities, and a noticeable gap in performance when translating to sub-systems. The development of substrate reuse methods and multi-junction cells

will likely alleviate some of these intrinsic trade-offs. Furthermore, novel approaches such as nano-structuring, spectral splitting, and near-field control may also help circumvent these issues. Several non-technical challenges also need be addressed. Namely, the field has yet to reach a consensus regarding efficiency testing and reporting, which would streamline the process of identifying favorable designs and recognizing new advances. Whether the full potential of TPVs will be reached – providing power on demand, near the point-of-use, and enabling greater integration of intermittent renewables – remains to be determined. Nonetheless, it appears that a substantial gain in performance is within reach if sufficient resources are devoted to overcoming the challenges outlined in this review.

Acknowledgements

This material is based upon work supported by the National Science Foundation under Grant No. IIP-1820395. The authors acknowledge Christine Wang for her input.

Author Contributions

Conceptualization, T.B., C.S., and A.L.; Methodology, T.B. and A.L.; Formal Analysis, T.B., C.S., and B.R.L.; Investigation, T.B. and C.S.; Writing – Original Draft, T.B., B.R.L., and A.L.; Writing – Review & Editing, T.B. and A.L.; Visualization, T.B.; Supervision, A.L.; Funding Acquisition, A.L.

Declaration of Interests

The authors declare no competing interests.

References

- 1. Fraas, L.M., Avery, J.E., and Huang, H.X. (2003). Thermophotovoltaic furnace—generator for the home using low bandgap GaSb cells. Semicond. Sci. Technol. *18*, S247–S253.
- 2. Bianchi, M., Ferrari, C., Melino, F., and Peretto, A. (2012). Feasibility study of a Thermo-Photo-Voltaic system for CHP application in residential buildings. Appl. Energy *97*, 704–713.
- 3. Durisch, W., and Bitnar, B. (2010). Novel thin film thermophotovoltaic system. Sol. Energy Mater. Sol. Cells *94*, 960–965.
- 4. Datas, A., Ramos, A., Martí, A., del Cañizo, C., and Luque, A. (2016). Ultra high temperature latent heat energy storage and thermophotovoltaic energy conversion. Energy *107*, 542–549.
- 5. Amy, C., Seyf, H.R., Steiner, M.A., Friedman, D.J., and Henry, A. (2019). Thermal energy grid storage using multi-junction photovoltaics. Energy Environ. Sci. *12*, 334–343.
- 6. Datas, A., and Martí, A. (2017). Thermophotovoltaic energy in space applications: Review and future potential. Sol. Energy Mater. Sol. Cells *161*, 285–296.
- 7. Licht, A., Pfiester, N., DeMeo, D., Chivers, J., and Vandervelde, T.E. (2019). A Review of Advances in Thermophotovoltaics for Power Generation and Waste Heat Harvesting. MRS Adv. *4*, 2271–2282.
- 8. Lenert, A., Bierman, D.M., Nam, Y., Chan, W.R., Celanović, I., Soljačić, M., and Wang, E.N. (2014). A nanophotonic solar thermophotovoltaic device. Nat. Nanotechnol. *9*, 126–130.
- 9. Harder, N.-P., and W rfel, P. (2003). Theoretical limits of thermophotovoltaic solar energy conversion. Semicond. Sci. Technol. *18*, S151–S157.
- 10. Ungaro, C., Gray, S.K., and Gupta, M.C. (2015). Solar thermophotovoltaic system using nanostructures. Opt. Express *23*, A1149–A1156.
- 11. Rephaeli, E., and Fan, S. (2009). Absorber and emitter for solar thermo-photovoltaic systems to achieve efficiency exceeding the Shockley-Queisser limit. Opt. Express *17*, 15145–15159.
- 12. Zhou, Z., Sakr, E., Sun, Y., and Bermel, P. (2016). Solar thermophotovoltaics: reshaping the solar spectrum. Nanophotonics *5*, 1–21.
- 13. Wang, Y., Liu, H., and Zhu, J. (2019). Solar thermophotovoltaics: Progress, challenges,

- and opportunities. APL Mater. 7, 080906.
- 14. Bierman, D.M., Lenert, A., Chan, W.R., Bhatia, B., Celanović, I., Soljačić, M., and Wang, E.N. (2016). Enhanced photovoltaic energy conversion using thermally based spectral shaping. Nat. Energy *1*, 16068.
- 15. Polman, A., Knight, M., Garnett, E.C., Ehrler, B., and Sinke, W.C. (2016). Photovoltaic materials: Present efficiencies and future challenges. Science (80-.). *352*, aad4424–aad4424.
- 16. Shockley, W., and Queisser, H.J. (1961). Detailed Balance Limit of Efficiency of p-n Junction Solar Cells. J. Appl. Phys. *32*, 510–519.
- 17. Green, M.A. (2006). Third generation photovoltaics: advanced solar energy conversion (Springer).
- 18. Mauk, M.G. (2006). Survey of Thermophotovoltaic (TPV) Devices. In Mid-infrared Semiconductor Optoelectronics (Springer London), pp. 673–738.
- 19. Ferrari, C., and Melino, F. (2014). Overview and Status of Thermophotovoltaic Systems. Energy Procedia *45*, 160–169.
- 20. Daneshvar, H., Prinja, R., and Kherani, N.P. (2015). Thermophotovoltaics: Fundamentals, challenges and prospects. Appl. Energy *159*, 560–575.
- Sakakibara, R., Stelmakh, V., Chan, W.R., Ghebrebrhan, M., Joannopoulos, J.D., Soljačić, M., and Čelanović, I. (2019). Practical emitters for thermophotovoltaics: a review. J. Photonics Energy 9, 032713.
- 22. Bhatt, R., Kravchenko, I., and Gupta, M. (2020). High-e ffi ciency solar thermophotovoltaic system using a nanostructure- based selective emitter. Sol. Energy 197, 538–545.
- 23. Fraas, L.M., Samaras, J.E., Huang, H.X., Minkin, L.M., Avery, J.E., Daniels, W.E., and Hui, S. (2001). TPV generators using the radiant tube burner configuration. Proc. 17 th Eur. PVSEC, Munich, Ger., 22–26.
- 24. Bitnar, B., Durisch, W., and Holzner, R. (2013). Thermophotovoltaics on the move to applications. Appl. Energy *105*, 430–438.
- Wilt, D., Chubb, D., Wolford, D., Magari, P., Crowley, C., Wilt, D., Chubb, D., Wolford, D., and Magari, P. (2007). Thermophotovoltaics for Space Power Applications. TPV7
 Seventh World ... 335, 335–345.

- 26. Suemitsu, M., Asano, T., Inoue, T., and Noda, S. (2020). High-Efficiency Thermophotovoltaic System That Employs an Emitter Based on a Silicon Rod-Type Photonic Crystal. ACS Photonics *7*, 80–87.
- 27. Mahorter, R.G., Wernsman, B., Thomas, R.M., and Siergiej, R.R. (2003). Thermophotovoltaic system testing. Semicond. Sci. Technol. *18*, S232–S238.
- 28. Bauer, T. (2011). Thermophotovoltaics: basic principles and critical aspects of system design (Springer Berlin Heidelberg).
- 29. Burger, T., Sempere, C., and Lenert, A. (2020). Thermophotovoltaic energy conversion: materials and device engineering. Nanoscale Energy Transp., 17-1-17–26.
- 30. Henry, C.H. (1980). Limiting efficiencies of ideal single and multiple energy gap terrestrial solar cells. J. Appl. Phys. *51*, 4494–4500.
- 31. Omair, Z., Scranton, G., Pazos-Outón, L.M., Xiao, T.P., Steiner, M.A., Ganapati, V., Peterson, P.F., Holzrichter, J., Atwater, H., and Yablonovitch, E. (2019). Ultraefficient thermophotovoltaic power conversion by band-edge spectral filtering. Proc. Natl. Acad. Sci. 116, 1–6.
- 32. Swanson, R.M. (1980). Recent developments in thermophotovoltaic conversion. In 1980 International Electron Devices Meeting (IRE), pp. 186–189.
- 33. Wernsman, B., Siergiej, R.R., Link, S.D., Mahorter, R.G., Palmisiano, M.N., Wehrer, R.J., Schultz, R.W., Schmuck, G.P., Messham, R.L., Murray, S., et al. (2004). Greater Than 20% Radiant Heat Conversion Efficiency of a Thermophotovoltaic Radiator/Module System Using Reflective Spectral Control. IEEE Trans. Electron Devices *51*, 512–515.
- 34. Woolf, D.N., Kadlec, E.A., Bethke, D., Grine, A.D., Nogan, J.J., Cederberg, J.G., Bruce Burckel, D., Luk, T.S., Shaner, E.A., and Hensley, J.M. (2018). High-efficiency thermophotovoltaic energy conversion enabled by a metamaterial selective emitter. Optica *5*, 213.
- Dashiell, M.W., Beausang, J.F., Ehsani, H., Nichols, G.J., Depoy, D.M., Danielson, L.R., Talamo, P., Rahner, K.D., Brown, E.J., Burger, S.R., et al. (2006). Quaternary InGaAsSb Thermophotovoltaic Diodes. IEEE Trans. Electron Devices 53, 2879–2891.
- 36. Fernández, J., Dimroth, F., Oliva, E., Hermle, M., and Bett, A.W. (2007). Back-surface Optimization of Germanium TPV Cells. In AIP Conference Proceedings (AIP), pp. 190–197.

- 37. Green, M.A., Hishikawa, Y., Dunlop, E.D., Levi, D.H., Hohl-Ebinger, J., Yoshita, M., and Ho-Baillie, A.W.Y. (2019). Solar cell efficiency tables (version 54). Prog. Photovoltaics Res. Appl. *27*, 3–12.
- 38. Haase, F., Hollemann, C., Schäfer, S., Merkle, A., Rienäcker, M., Krügener, J., Brendel, R., and Peibst, R. (2018). Laser contact openings for local poly-Si-metal contacts enabling 26.1%-efficient POLO-IBC solar cells. Sol. Energy Mater. Sol. Cells *186*, 184–193.
- 39. Yoshikawa, K., Kawasaki, H., Yoshida, W., Irie, T., Konishi, K., Nakano, K., Uto, T., Adachi, D., Kanematsu, M., Uzu, H., et al. (2017). Silicon heterojunction solar cell with interdigitated back contacts for a photoconversion efficiency over 26%. Nat. Energy *2*, 17032.
- 40. Kayes, B.M., Nie, H., Twist, R., Spruytte, S.G., Reinhardt, F., Kizilyalli, I.C., and Higashi, G.S. (2011). 27.6% Conversion efficiency, a new record for single-junction solar cells under 1 sun illumination. In 2011 37th IEEE Photovoltaic Specialists Conference (IEEE), pp. 000004–000008.
- 41. Geisz, J.F., Steiner, M.A., García, I., Kurtz, S.R., and Friedman, D.J. (2013). Enhanced external radiative efficiency for 20.8% efficient single-junction GaInP solar cells. Appl. Phys. Lett. *103*, 1–5.
- 42. Wilt, D.M., Fatemi, N.S., Hoffman, R.W., Jenkins, P.P., Scheiman, D., Lowe, R., Landis, G.A., Fatemi, S., Hoffman, R.W., Jenkins, P.P., et al. (1995). Ingaas Pv Device Development for Tpv Power Systems. First Nrel Conf. Theromophotovoltic Gener. Electr., 210–220.
- 43. Cederberg, J.G., Blaich, J.D., Girard, G.R., Lee, S.R., Nelson, D.P., and Murray, C.S. (2008). The development of (InGa)As thermophotovoltaic cells on InP using strain-relaxed In(PAs) buffers. J. Cryst. Growth *310*, 3453–3458.
- 44. Rinnerbauer, V., Ndao, S., Yeng, Y.X., Chan, W.R., Senkevich, J.J., Joannopoulos, J.D., Soljačić, M., and Celanovic, I. (2012). Recent developments in high-temperature photonic crystals for energy conversion. Energy Environ. Sci. *5*, 8815.
- 45. Nakagawa, N., Ohtsubo, H., Waku, Y., and Yugami, H. (2005). Thermal emission properties of Al2O3/Er3Al5O12 eutectic ceramics. J. Eur. Ceram. Soc. *25*, 1285–1291.
- 46. Yeng, Y.X., Ghebrebrhan, M., Bermel, P., Chan, W.R., Joannopoulos, J.D., Soljacic, M., and Celanovic, I. (2012). Enabling high-temperature nanophotonics for energy

- applications. Proc. Natl. Acad. Sci. 109, 2280–2285.
- 47. Burger, T., Fan, D., Lee, K., Forrest, S.R., and Lenert, A. (2018). Thin-Film Architectures with High Spectral Selectivity for Thermophotovoltaic Cells. ACS Photonics *5*, 2748–2754.
- 48. Shemelya, C., Demeo, D.F., and Vandervelde, T.E. (2014). Two dimensional metallic photonic crystals for light trapping and anti-reflective coatings in thermophotovoltaic applications. Appl. Phys. Lett. *104*, 1–4.
- 49. Arpin, K.A., Losego, M.D., Cloud, A.N., Ning, H., Mallek, J., Sergeant, N.P., Zhu, L., Yu, Z., Kalanyan, B., Parsons, G.N., et al. (2013). Three-dimensional self-assembled photonic crystals with high temperature stability for thermal emission modification. Nat. Commun. *4*, 2630.
- 50. Cao, F., Kraemer, D., Tang, L., Li, Y., Litvinchuk, A.P., Bao, J., Chen, G., and Ren, Z. (2015). A high-performance spectrally-selective solar absorber based on a yttria-stabilized zirconia cermet with high-temperature stability. Energy Environ. Sci. 8, 3040–3048.
- 51. Baranov, D.G., Xiao, Y., Nechepurenko, I.A., Krasnok, A., Alù, A., and Kats, M.A. (2019). Nanophotonic engineering of far-field thermal emitters. Nat. Mater. *18*, 920–930.
- 52. Ferguson, L.G., and Dogan, F. (2001). A highly efficient NiO-Doped MgO matched emitter for thermophotovoltaic energy conversion. Mater. Sci. Eng. B *83*, 35–41.
- Rinnerbauer, V., Yeng, Y.X., Chan, W.R., Senkevich, J.J., Joannopoulos, J.D., Soljačić,
 M., and Celanovic, I. (2013). High-temperature stability and selective thermal emission of polycrystalline tantalum photonic crystals. Opt. Express 21, 11482.
- Wang, Y., Zhou, L., Zhang, Y., Yu, J., Huang, B., Wang, Y., Lai, Y., Zhu, S., and Zhu, J.
 (2018). Hybrid Solar Absorber-Emitter by Coherence-Enhanced Absorption for Improved
 Solar Thermophotovoltaic Conversion. Adv. Opt. Mater. 6, 1800813.
- 55. Chirumamilla, M., Krishnamurthy, G.V., Knopp, K., Krekeler, T., Graf, M., Jalas, D., Ritter, M., Störmer, M., Petrov, A.Y., and Eich, M. (2019). Metamaterial emitter for thermophotovoltaics stable up to 1400 °C. Sci. Rep. *9*, 7241.
- 56. Chirumamilla, M., Krishnamurthy, G.V., Rout, S.S., Ritter, M., Störmer, M., Petrov, A.Y., and Eich, M. (2020). Thermal stability of tungsten based metamaterial emitter under medium vacuum and inert gas conditions. Sci. Rep. *10*, 2–11.
- 57. Nagpal, P., Josephson, D.P., Denny, N.R., DeWilde, J., Norris, D.J., and Stein, A. (2011).

- Fabrication of carbon/refractory metal nanocomposites as thermally stable metallic photonic crystals. J. Mater. Chem. *21*, 10836.
- 58. Thermal stability of micro-structured selective W emitters (Schlemmer).pdf.
- 59. Arpin, K.A., Losego, M.D., and Braun, P. V. (2011). Electrodeposited 3D tungsten photonic crystals with enhanced thermal stability. Chem. Mater. *23*, 4783–4788.
- 60. Lee, H.J., Smyth, K., Bathurst, S., Chou, J., Ghebrebrhan, M., Joannopoulos, J., Saka, N., and Kim, S.G. (2013). Hafnia-plugged microcavities for thermal stability of selective emitters. Appl. Phys. Lett. *102*, 1–5.
- 61. Peykov, D., Yeng, Y.X., Celanovic, I., Joannopoulos, J.D., and Schuh, C.A. (2015). Effects of surface diffusion on high temperature selective emitters. Opt. Express *23*, 9979.
- 62. Abbas, R., Muñoz, J., and Martínez-Val, J.M. (2012). Steady-state thermal analysis of an innovative receiver for linear Fresnel reflectors. Appl. Energy *92*, 503–515.
- 63. Bitnar, S., Durisch, W., Palfinger, G., von Roth, F., Vogt, U., Brönstrup, A., and Seiler, D. (2004). Practical thermophotovoltaic generators. Semiconductors *38*, 941–945.
- 64. Raman, V.K., Burger, T., and Lenert, A. (2019). Design of thermophotovoltaics for tolerance of parasitic absorption. Opt. Express *27*, 31757.
- 65. Baldasaro, P.F., Raynolds, J.E., Charache, G.W., DePoy, D.M., Ballinger, C.T., Donovan, T., and Borrego, J.M. (2001). Thermodynamic analysis of thermophotovoltaic efficiency and power density tradeoffs. J. Appl. Phys. 89, 3319–3327.
- 66. Wang, C. a, Shiau, D. a, Murphy, P.G., O'Brien, P.W., Huang, R.K., Connors, M.K., Anderson, a C., Donetsky, D., Anikeev, S., Belenky, G., et al. (2004). Wafer bonding and epitaxial transfer of GaSb-based epitaxy to GaAs for monolithic interconnection of thermophotovoltaic devices. J. Electron. Mater. *33*, 213–217.
- 67. Wu, X., Duda, A., Carapella, J.J., Ward, J.S., Webb, J.D., and Wanlass, M.W. (1999). A Study of Contacts and Back-Surface Reflectors Interconnected Modules. *517*.
- Shvarts, M.Z.Z., Andreev, V.M.M., Khvostikov, V.P.P., Rumyantsev, V.D.D., Sorokina, S.V., Vasil'ev, V.I., Vlasov, A.S., Chosta, O.I., Larinov, V.R., and Rumyantsev, V.D.D. (1998). GaSb/InGaAsSb tandem thermophotovoltaic cells for space applications. Proc. Fifth Eur. Sp. Power Conf., 527.
- 69. Siergiej, R.R., Sinharoy, S., Valko, T., Wehrer, R.J., Wernsman, B., Link, S.D., Schultz, R.W., and Messham, R.L. (2004). InGaAsP/InGaAs Tandem TPV Device. In AIP

- Conference Proceedings (AIP), pp. 480–488.
- Andreev, V.M., Khvostikov, V.P., Rumyantsev, V.D., Sorokina, S. V., and Shvarts, M.Z. (2000). Single-junction GaSb and tandem GaSb/InGaAsSb & AlGaAsSb/GaSb thermophotovoltaic cells. Conf. Rec. IEEE Photovolt. Spec. Conf. 2000-Janua, 1265–1268.
- 71. Wehrer, R., Wanlass, M., Wilt, D., Wernsman, B., Siergiej, R., and Carapella, J. (2003). InGaAs series-connected, tandem, MIM TPV converters. Proc. 3rd World Conf. Photovolt. Energy Convers. *A*, 892–895.
- 72. Siergiej, R.R., Wernsman, B., Derry, S.A., Wehrer, R.J., Link, S.D., Palmisiano, M.N., Riley, D.R., Murray, C.S., Newman, F., and Hills, J. (2000). High efficiency, large area, InGaAs/InPAs thermophotovoltaic cells. In Device Research Conference. Conference Digest (Cat. No.01TH8561) (IEEE), pp. 159–160.
- 73. Datas, A. (2015). Optimum semiconductor bandgaps in single junction and multijunction thermophotovoltaic converters. Sol. Energy Mater. Sol. Cells *134*, 275–290.
- 74. Steiner, M.A., Geisz, J.F., García, I., Friedman, D.J., Duda, A., and Kurtz, S.R. (2013). Optical enhancement of the open-circuit voltage in high quality GaAs solar cells. J. Appl. Phys. *113*, 123109.
- 75. Schilling, C.L., Hohn, O., Micha, D.N., Heckelmann, S., Klinger, V., Oliva, E., Glunz, S.W., and Dimroth, F. (2018). Combining Photon Recycling and Concentrated Illumination in a GaAs Heterojunction Solar Cell. IEEE J. Photovoltaics *8*, 348–354.
- 76. Miller, O.D., Yablonovitch, E., and Kurtz, S.R. (2012). Strong Internal and External Luminescence as Solar Cells Approach the Shockley–Queisser Limit. IEEE J. Photovoltaics *2*, 303–311.
- 77. Kosten, E.D., Atwater, J.H., Parsons, J., Polman, A., and Atwater, H.A. (2013). Highly efficient GaAs solar cells by limiting light emission angle. Light Sci. Appl. *2*, 1–6.
- 78. Kuang, Y., Vece, M. Di, Rath, J.K., Wu, C., Iii, B.N., John, J., Kowalczewski, P., Redorici, L., Bozzola, A., Albrecht, S., et al. Roadmap on optical energy conversion.
- 79. Algora, C. (2003). Modelling And Manufacturing GaSb TPV Converters. 452–461.
- 80. Tang, L., Fraas, L.M., Liu, Z., Xu, C., and Chen, X. (2015). Performance Improvement of the GaSb Thermophotovoltaic Cells With n-Type Emitters. IEEE Trans. Electron Devices 62, 2809–2815.

- 81. Tang, L., Fraas, L.M., Liu, Z., Zhang, Y., Duan, H., and Xu, C. (2019). N-type vapor diffusion for the fabrication of GaSb thermophotovoltaic cells to increase the quantum efficiency in the long wavelength range. Sol. Energy Mater. Sol. Cells *194*, 137–141.
- 82. Molesky, S., and Jacob, Z. (2015). Ideal near-field thermophotovoltaic cells. Phys. Rev. B Condens. Matter Mater. Phys. *91*, 1–7.
- 83. Chen, K., Santhanam, P., and Fan, S. (2015). Suppressing sub-bandgap phonon-polariton heat transfer in near-field thermophotovoltaic devices for waste heat recovery. Appl. Phys. Lett. *107*, 091106.
- 84. Fiorino, A., Zhu, L., Thompson, D., Mittapally, R., Reddy, P., and Meyhofer, E. (2018). Nanogap near-field thermophotovoltaics. Nat. Nanotechnol. *13*, 806–811.
- 85. Tervo, E., Bagherisereshki, E., and Zhang, Z. (2018). Near-field radiative thermoelectric energy converters: a review. Front. Energy *12*, 5–21.
- 86. DeSutter, J., Tang, L., and Francoeur, M. (2019). A near-field radiative heat transfer device. Nat. Nanotechnol. *14*, 751–755.
- 87. McSherry, S., Burger, T., and Lenert, A. (2019). Effects of narrowband transport on near-field and far-field thermophotonic conversion. J. Photonics Energy *9*, 1.
- 88. Papadakis, G.T., Buddhiraju, S., Zhao, Z., Zhao, B., and Fan, S. (2020). Broadening near-field emission performance enhancement in thermophotovoltaics. Nano Lett.
- 89. Blandre, E., Vaillon, R., and Drévillon, J. (2019). New insights into the thermal behavior and management of thermophotovoltaic systems. Opt. Express *27*, 36340.
- 90. Stark, A.K., and Klausner, J.F. (2017). An R&D Strategy to Decouple Energy from Water. Joule *1*, 416–420.
- 91. Wen, R., Ma, X., Lee, Y.C., and Yang, R. (2018). Liquid-Vapor Phase-Change Heat Transfer on Functionalized Nanowired Surfaces and Beyond. Joule *2*, 2307–2347.
- 92. Weinstein, L.A., McEnaney, K., Strobach, E., Yang, S., Bhatia, B., Zhao, L., Huang, Y., Loomis, J., Cao, F., Boriskina, S. V., et al. (2018). A Hybrid Electric and Thermal Solar Receiver. Joule *2*, 962–975.
- 93. Crowley, C.J., Elkouh, N.A., Murray, S., and Chubb, D.L. (2005). Thermophotovoltaic Converter Performance for Radioisotope Power Systems. In AIP Conference Proceedings (AIP), pp. 601–614.
- 94. Yeng, Y.X., Chan, W.R., Rinnerbauer, V., Stelmakh, V., Senkevich, J.J., Joannopoulos,

- J.D., Soljacic, M., and Čelanović, I. (2015). Photonic crystal enhanced silicon cell based thermophotovoltaic systems. Opt. Express *23*, A157.
- 95. Wilt, D., Wehrer, R., Palmisiano, M., Wanlass, M., and Murray, C. (2003). Monolithic interconnected modules (MIMs) for thermophotovoltaic energy conversion. *18*.
- 96. Horowitz, K.A., Remo, T.W., Smith, B., and Ptak, A.J. (2018). A Techno-Economic Analysis and Cost Reduction Roadmap for III-V Solar Cells.
- 97. Lee, K., Zimmerman, J.D., Hughes, T.W., and Forrest, S.R. (2014). Non-Destructive Wafer Recycling for Low-Cost Thin-Film Flexible Optoelectronics. Adv. Funct. Mater. *24*, 4284–4291.
- 98. Lee, K., Shiu, K.T., Zimmerman, J.D., Renshaw, C.K., and Forrest, S.R. (2010). Multiple growths of epitaxial lift-off solar cells from a single InP substrate. Appl. Phys. Lett. *97*, 10–12.
- 99. Brown, E., Baldasar, P., Danielson, L., DePoy, D., Dolatowski, J., Fourspring, P.M., Nichols, G., Topper, W., and Rahmlow, T. (2004). The Status of Thermophotovoltaic Energy Conversion Technology at Lockheed Martin Corp. *06478*, 1–20.
- 100. Yu, Y.Z., Martinelli, R.U., Taylor, G.C., Shellenbarger, Z., Smeltzer, R.K., Li, J., Palit, K., Burger, S.R., Cardines, R.P., Danielson, L.R., et al. (2003). High-Efficiency Multi-Cell TPV Module Fabrication and Performance. AIP Conf. Proc. 653, 335–343.
- 101. Siergiej, R.R., Wernsman, B., Derry, S.A., Mahorter, R.G., Wehrer, R.J., Link, S.D., Palmisiano, M.N., Messham, R.L., Murray, S., Murray, C.S., et al. (2003). 20% Efficient InGaAs/InPAs Thermophotovoltaic Cells. In AIP Conference Proceedings (AIP), pp. 414–423.
- 102. Wedlock, B.D. (1963). Thermo-photo-voltaic energy conversion. Proc. IEEE *51*, 694–698.
- 103. Swanson, R.M. (1978). Silicon photovoltaic cells in thermophotovoltaic energy conversion. In 1978 International Electron Devices Meeting (IRE), pp. 70–73.

Figure captions

- Figure 1. Energy transport and conversion in a thermophotovoltaic generator. Upstream conversion of an energy source heats the thermal emitter, generating radiation that interacts with the cell. Photoexcitation (by in-band radiation) and separation of charge carriers in the cell enables power generation (P_{out}). A portion of incident radiation is reflected by the cell and returned to the emitter (i.e., photon recycling/recuperation). Q_h denotes net energy flow out of the emitter and Q_{abs} denotes radiation absorbed at the cell. Loss pathways within the TPV sub-system include (i) emission to non-current-generating surfaces in the cavity (e.g., edges, contact lines, etc.) and convective loss from the emitter, and (ii) cell inefficiencies, such as thermalization, non-radiative recombination, out-of-band absorption, and Ohmic losses. Upstream inefficiencies related to conversion of the energy source and heat transfer to the emitter depend on the source and are not attributed to the TPV sub-system in this work.
- **Figure 2. Record pairwise efficiencies spanning cell materials**. (a) Absolute efficiencies as reported. (b) Efficiencies normalized against the radiative limit. Reporting literature: InGaAsSb³⁵; 0.6 eV InGaAs³⁴; Ge³⁶; GaSb²³; LM InGaAs³¹ (triangular markers); Si.³²
- **Figure 3. Characteristics and limitations of leading TPV pairs.** (a) The product of *SE* and *IQE* describes the quality of spectral management. *VF* and *FF* characterize the effectiveness of charge carrier management. Normalization to corresponding values in the radiative limit provides a basis for identifying target metrics for improvement. (b-d) Reported, absolute performance metrics. (e-g) Performance metrics, normalized to corresponding values in the radiative limit. Reporting literature: InGaAsSb³⁵; 0.6 eV InGaAs³⁴; Ge³⁶; GaSb²³; LM InGaAs³¹ (triangular markers); Si.³²
- Figure 4. Component-wise spectral control strategies. Individual spectral efficiencies of (a) selective emitters and (d) selectively absorptive cells. Experimental values are compared to SE curves for various out-of-band emissivities with ideal in-band absorption ($\varepsilon_{in} = 1$). Examples of spectral control structures: (b) Al₂O₃/Er₃Al₅O₁₂ eutectic ceramic, ⁴⁵ (c) 2D W cavity array, ⁴⁶ (e) thin-film LM InGaAs with Au BSR, ⁴⁷ (f) 2D photonic crystal front-surface filter on a GaSb cell. ⁴⁸
- **Figure 5. Effective dark current density of leading TPV cells.** Radiative limit dark current density with (solid curve) and without (dashed curve) internal photon recycling. Reporting literature: InGaAsSb³⁵; 0.6 eV InGaAs³⁴; Ge³⁶; GaSb²³; LM InGaAs³¹ (triangular marker); Si.³²
- **Figure 6. Gaps between pairwise and TPV sub-system efficiencies**. Leading pairwise cell efficiencies compared to record sub-system efficiencies. Reporting literature: InGaAsSb^{14,35}; 0.6 eV InGaAs^{34,93}; Ge³⁶; GaSb^{22,23}; LM InGaAs^{26,31} (triangular marker); Si.^{32,94}
- Figure C1. Performance metric calculations as a function of cutoff energy. Example emittercell pair has $T_h = 1500 \text{ K}$, $T_c = 293 \text{ K}$, $\varepsilon_{in} = 1$, $\varepsilon_{out} = 0.05$, and fixed J_{sc} .